

International Journal of Modern Physics E
 © World Scientific Publishing Company

NONMESONIC WEAK DECAY DYNAMICS FROM PROTON SPECTRA OF Λ -HYPERNUCLEI

FRANJO KRMPOTIĆ

*Instituto de Física La Plata, Universidad Nacional de La Plata
 1900 La Plata, Argentina*

*Instituto de Física Teórica, UNESP - Univ. Estadual Paulista,
 São Paulo, São Paulo 01140-070, Brasil
 krmpotic@fisica.unlp.edu.ar*

CLÁUDIO DE CONTI

*Campus Experimental de Itapeva, UNESP - Univ Estadual Paulista,
 Itapeva, São Paulo 18409-110, Brasil
 conti@itapeva.unesp.br*

A novel comparison between the data and the theory is proposed for the nonmesonic (NM) weak decay of hypernuclei. Instead of confronting the primary decay rates, as is usually done, we focus attention on the effective decay rates that are straightforwardly related with the number of emitted particles. Proton kinetic energy spectra of ${}^5_{\Lambda}\text{He}$, ${}^7_{\Lambda}\text{Li}$, ${}^9_{\Lambda}\text{Be}$, ${}^{11}_{\Lambda}\text{B}$, ${}^{12}_{\Lambda}\text{C}$, ${}^{13}_{\Lambda}\text{C}$, ${}^{15}_{\Lambda}\text{N}$ and ${}^{16}_{\Lambda}\text{O}$, measured by FINUDA, are evaluated theoretically. The Independent Particle Shell Model (IPSM) is used as the nuclear structure framework, while the dynamics is described by the One-Meson-Exchange (OME) potential. Only for the ${}^5_{\Lambda}\text{He}$, ${}^7_{\Lambda}\text{Li}$, and ${}^{12}_{\Lambda}\text{C}$ hypernuclei is it possible to make a comparison with the data, since for the rest there is no published experimental information on number of produced hypernuclei. Considering solely the one-nucleon-induced ($1N$ -NM) decay channel, the theory reproduces correctly the shapes of all three spectra at medium and high energies ($E_p \gtrsim 40$ MeV). Yet, it greatly overestimates their magnitudes, as well as the corresponding transition rates when the full OME ($\pi + K + \eta + \rho + \omega + K^*$) model is used. The agreement is much improved when only the $\pi + K$ mesons with soft dipole cutoff parameters participate in the decay process. We find that the IPSM is a fair first order approximation to disentangle the dynamics of the $1N$ -NM decay, the knowledge of which is indispensable to inquire about the baryon-baryon strangeness-flipping interaction. It is shown that the IPSM provides very useful insights regarding the determination the $2N$ -NM decay rate. In a new analysis of the FINUDA data, we derive two results for this quantity with one of them close to that obtained previously.

Keywords: Hypernuclei; Hyperon-nucleon interaction; Nuclear structure models and methods.

PACS numbers: 21.80.+a, 13.75.Ev, 21.60.-n

1. Introduction

The weak decay rate of a Λ hypernucleus can be expressed as¹

$$\Gamma_W = \Gamma_M + \Gamma_{NM}, \quad (1)$$

where Γ_M is the decay rate for the mesonic (M) decay $\Lambda \rightarrow \pi N$, and Γ_{NM} is the rate for the nonmesonic (NM) decay, which can be induced either by one bound nucleon ($1N$), $\Gamma_1^0(\Lambda N \rightarrow nN)$, or by two bound nucleons ($2N$), $\Gamma_2^0(\Lambda NN \rightarrow nNN)$, or even more bound nucleons *i.e.*,

$$\Gamma_{NM} = \Gamma_1^0 + \Gamma_2^0 + \dots; \quad \Gamma_1^0 = \Gamma_p^0 + \Gamma_n^0, \quad \Gamma_2^0 = \Gamma_{nn}^0 + \Gamma_{np}^0 + \Gamma_{pp}^0. \quad (2)$$

With the symbol \dots we indicate that additional processes, such as those induced by three nucleons, can contribute also. We use the superscript 0 to distinguish between the primary (bare) decay rates, and the effective decay rates

$$\begin{aligned} \Gamma_p &= \Gamma_p^{0,FSI} + \Gamma_n^{0,FSI} + \Gamma_{np}^{0,FSI} + 2\Gamma_{pp}^{0,FSI} + \dots, \\ \Gamma_n &= \Gamma_p^{0,FSI} + 2\Gamma_n^{0,FSI} + 2\Gamma_{np}^{0,FSI} + \Gamma_{pp}^{0,FSI} + 3\Gamma_{nn}^{0,FSI} + \dots, \\ \Gamma_{np} &= \Gamma_p^{0,FSI} + 2\Gamma_{np}^{0,FSI} + 2\Gamma_{pp}^{0,FSI} + \dots, \\ \Gamma_{nn} &= \Gamma_n^{0,FSI} + 3\Gamma_{nn}^{0,FSI} + \Gamma_{np}^{0,FSI} + \dots. \end{aligned} \quad (3)$$

which are affected by final state interactions (FSIs) and are directly related to the numbers of measured single-nucleons N_N , and two-particle coincidences N_{nN} , as

$$\Gamma_N = \frac{\Gamma_W}{N_W} N_N, \quad \Gamma_{nN} = \frac{\Gamma_W}{N_W} N_{nN}, \quad (4)$$

where the number of produced hypernuclei N_W and the corresponding decay rate Γ_W are experimentally measured quantities. The primary nucleons, in propagating within the nuclear environment, interact with the surrounding nucleons representing a complicated many-body problem generically designated as FSIs. In Eq. (3) we have considered only the dominant primary decays that are later perturbed by FSIs, and this is the meaning of $+\dots$.

The schematic representation of the two decay channels, when the pertinent dynamics is described by one-meson-exchange (OME) potentials, is shown in Fig. 1. This is the most frequently used model for handling the NM-decay, including usually the exchanges of nonstrange-mesons π, ρ, ω , and η , and strange-mesons K , and K^* . It is based on the original idea of Yukawa that the NN interaction at long distance is due to the one-pion-exchange (OPE), with the dominant role played by the exchange of pion and kaon mesons.

The OPE potential was verified quantitatively by the Nijmegen partial wave analysis of NN scattering in the elastic region,² *i.e.*, at distances larger than the minimal de Broglie wavelength $1/\sqrt{m_\pi M} \sim 0.5$ fm corresponding to the pion production threshold. The verification of other meson exchanges is less straightforward, and the uncertainties in the baryon-baryon-meson (BBM) coupling constants could be sizeable since they are not constrained by experiments. To derive them in the strong sector (S vertices in Fig. 1), the $SU(3)_f$ (flavor) symmetry is utilized. In

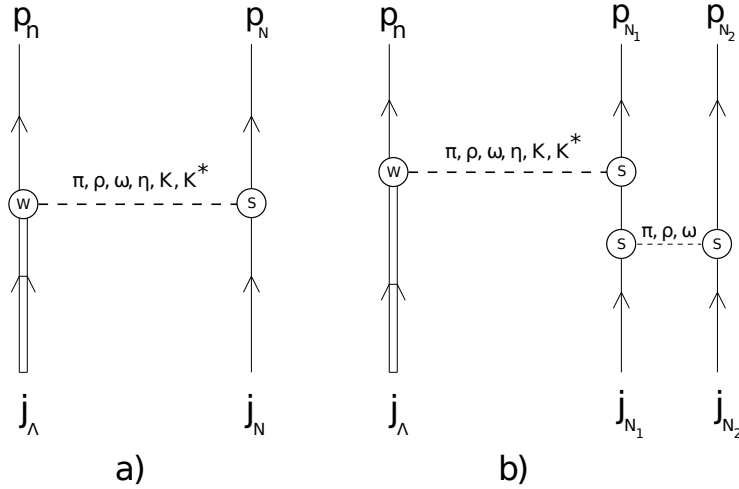


Fig. 1. Schematic representation of a) one-nucleon, and b) two-nucleon induced decays in Λ -hypernuclei when described by the interplay of weak (W) and strong (S) interactions through the exchanges of nonstrange-mesons π, ρ, ω , and η , and strange-mesons K , and K^* . The W and S vertices are exchanged for strange mesons.

the weak sector (W vertex in Fig. 1), the BBM parity-violating couplings are obtained from the $SU(6)_W$ (weak) symmetry, while the parity conserving couplings are derived from a pole-model with only baryon pole resonances.^{3,4}

The BBM vertex functions also involve uncertainties in the dipole cutoff parameters Λ_M which, being off-shell quantities, can not be determined experimentally. We only know that, to have a physical meaning, they have to be of hadronic scale (~ 1 GeV). For instance, in different calculations, the Λ_π for the off-shell pion varies from 0.7 to 1.3 GeV.³⁻⁹ In particular, the pion cutoffs of 1.2 GeV, and 0.8 GeV were used to describe the electromagnetically induced two-nucleon emission processes (γ, pn) and (γ, pp) ,⁷ which are quite similar to the $1N$ -NM decays $(\Lambda p, np)$, and $(\Lambda n, nn)$. We use here the Λ_M 's from Ref.,⁴ and also those proposed in Ref.^{8,9} to account for the transition rates Γ_p and Γ_n in the s -shell hypernuclei.^a

The short-range correlations (SRCs) between the emitted nucleons nN , and nNN can also affect significantly the BBM couplings. Parreño and Ramos have shown that they can diminish the value of Γ_1^0 by more than a factor of two.¹¹ Nothing has been stated so far regarding the effect of the SRCs on the $2N$ -NM decay. The theoretical scene becomes even more complex when effects of the quark degrees of freedom,^{12,13} the 2π -exchanges,¹⁴⁻¹⁷ and the axial-vector a_1 -meson exchange^{16,17} are considered.

The M and $1N$ -NM decays have been observed experimentally in the pioneering

^a The dependence of the NMWD transition rates on the values of Λ_M , and therefore on the BBM vertex functions, is thoroughly discussed in Table 1 and Fig. 1 of Ref.⁸

measurement performed more than 50 years ago by Ruderman and R. Karplus.¹⁸ Conversely, the experimental observation of the $2N$ -NM decay, which was predicted by Alberico *et al.*¹⁹ in 1991 (see also Ref.²⁰), has been reported only in recent years at KEK,²¹ and at FINUDA.^{22–24} Both groups announced a branching ratio $\Gamma_2^0/\Gamma_{NM} \sim 25 - 30$ %. The first group obtained this result from the single and double coincidence nucleon spectra in $^{12}_\Lambda\text{C}$, and the second one from proton kinetic energy spectra in $^5_\Lambda\text{He}$, $^7_\Lambda\text{Li}$, $^9_\Lambda\text{Be}$, $^{11}_\Lambda\text{B}$, $^{12}_\Lambda\text{C}$, $^{13}_\Lambda\text{C}$, $^{15}_\Lambda\text{N}$ and $^{16}_\Lambda\text{O}$. A branching ratio for the $2N$ -NM decay channel of this magnitude is consistent with the prediction made by Bauer and Garbarino.²⁵ On the other hand, the one-particle proton and neutron kinetic energy spectra in $^4_\Lambda\text{He}$ measured at BNL²⁶ are accounted for reasonably well theoretically by considering only the $1N$ -NM decay mode.^{8,9}

The above mentioned experiments, together with several others performed during the last few decades,^{23,27–35} represent very important advances in our knowledge about NM decay. Explicitly, these advances are: 1) new high quality measurements of the number of single-nucleons N_N , as a function of the one-nucleon energy E_N , and 2) first measurements of the number of two-particle coincidences N_{nN} , as a function of: i) the sum of the kinetic energies $E_{nN} \equiv E_n + E_N$, ii) the opening angle θ_{nN} , and iii) the center of mass (c.m.) momentum $P_{nN} = |\mathbf{p}_n + \mathbf{p}_N|$. On the theoretical side this implies a new challenge for nuclear models which have to explain, not only the $1N$ - and $2N$ -NM decay rates, but also the shapes and magnitudes of all these spectra, testing in this way both the kinematics and the dynamics.

Recently, Bauer, Garbarino, Parreño and Ramos^{36–38} have obtained good agreement with KEK data,²¹ considering both the one- and the two-nucleon induced decays in the framework of the Fermi Gas Model (FGM). These authors have also analyzed the proton kinetic energy spectrum in $^{12}_\Lambda\text{C}$ measured at FINUDA,²⁴ but no theoretical analysis of the remaining spectra has been done so far. In the present work, we present for the first time the calculation of all proton kinetic energy spectra studied in the above mentioned experiment.

Since i) the NMWD is dominated by the $1N$ -NM decay, and ii) the $2N$ -NM processes and the FSIs contribute mainly at low energy, it is reasonable and useful to compare the experimental spectra with theoretical calculation when only the $1N$ -NM decay mode is considered.^b It is obvious that there will be no agreement at low energies between the experimental and theoretical spectra. But this disagreement is not crucially important, since we are basically interested in disentangling the strangeness-flipping interaction among baryons.⁹ Of course, both the $2N$ -NM decay and the FSIs, as well as the SRCs, are interesting physical phenomena in themselves,

^b Such a comparison is analogous to those done between the experimental data on electron-nucleus and charged-current neutrino-nucleus scatterings that include the FSIs, with the plane-wave impulse approximation which doesn't include these processes.^{39,40} Moreover, the results of our analysis are fully robust, in the sense that they will be valid even after the inclusion of the FSIs and the $2N$ -NM decay.

but they teach us little about the basic nonmesonic decay. Moreover, as indicated in (3) they can not be treated separately, and it is not known whether they contribute coherently or incoherently. That is, it can even happen that they partially cancel out (for instance, $\Gamma_n^{0,FSI}$ and $\Gamma_{np}^{0,FSI}$ terms in (3)), as do the divergences and the vertex corrections in the QED, because of Ward identity. More specifically, and as already pointed out in Ref.,¹⁰ the issue of FSIs in the NMWD is a tough nut to crack, and there is no theoretical work in the literature encompassing all aspects of these processes. For this reason, before having a reasonable control over all the physics that they involve, it may be useful, or even preferable, to discuss the experimental data without the FSIs. This is what we do here.

The content of this article is as follows. Our method to compare the experimental data with theory for the NMWD is explained in detail in Sec. 2. The main formulas used to calculate the proton spectra for the $1N$ -NM decay within the Independent-Particle Shell Model (IPSM) is presented in Sec. 3. The parameterizations that are used for vertices are listed in Sec. 3 also. The only novelty here is that the proposed BBM vertex functions are rarely used in the literature. The calculated spectra for all hypernuclei are presented in Sec. 4, where we make a comparison between theory and the FINUDA data for ${}^5_{\Lambda}\text{He}$, ${}^7_{\Lambda}\text{Li}$, and ${}^{12}_{\Lambda}\text{C}$. The extraction of Γ_2^0 from experimental spectra is reanalyzed in Sec. 5. Finally, Sec. 6 presents the final remarks and conclusions.

2. Relationship between Experiment and Theory

While Γ_N and Γ_{nN} are experimentally observable quantities, the bare decay rates Γ_p^0 , Γ_n^0 , and Γ_2^0 are not and have to be derived from the data, employing different extraction procedures which frequently involve approximations that are questionable. (One example will be illustrated here.) Moreover, the primary decay rates are ill defined, since they depend on the model that is used to describe the nuclear structure of the hypernucleus, as well as on the SRC, etc.

Note that we include the FSIs in the definition of Γ_N , and Γ_{nN} which is not commonly done in the study of the NMWD.^{10,37} But, there are other processes in nuclear physics where the FSIs participate in the definition of the decay rates. The best known phenomenon is nuclear β -decay, where the transition rate depends on the FSIs caused by the Coulomb attraction of the emitted electrons. (See, for instance, Eq. (5.11) in Ref.⁴¹ where the FSIs effects are approximated by the Fermi function.) The main difference between the FSIs in the leptonic and nonmesonic weak-decays is that while in the first case they are easily evaluated, in the second case they are very complicated¹⁰ and beyond the scope of this work.

The FSIs are usually simulated by a semi-classical model, developed by Ramos *et al.*,⁴² and denominated Intranuclear Cascade (INC) code. This code interrelates the primary rates (2) with measured rates (3). More recently, the FSIs were evaluated with a time-dependent multicollisional Monte Carlo cascade scheme,^{43,44} implemented within the CRISP code (Collaboration Rio-Sao Paulo), which describes,

in a phenomenological way, both the nucleon-nucleon scattering inside the nucleus and the escape of nucleons from the nuclear surface.^{45–48} The CRISP code, as all INC codes, is tailored to simulate the experimental data, and not for describing theoretically the FSIs. As such, it involves a normalization procedure for the experimental data, which washes out all of the information on the NMWD dynamics. More specifically, the spectra of Γ_1^0 evaluated from a Shell Model (SM) are the main ingredients for establishing the initial condition to start the CRISP cascade process and to calculate in this way the FSIs. (The primary spectra of Γ_2^0 should also be included within the initial conditions in a more complete model, but we do not know yet how are they evaluated within the SM.) Yet, because of the normalization, the spectrum perturbed by the FSIs turns out to be the same for different primary spectra. (One obtains the same $\Gamma_p^{0,FSI}$ spectra for different Γ_p^0 spectra, etc.) We were not able, so far, to find out how to circumvent this problem of normalization. Moreover, not all FSIs are considered within the INC codes. Which additional FSIs contribute to the NMWD spectra and decay rates, and how and which of them should be included in the calculation are nontrivial questions. Some candidates are discussed in Ref.¹⁰

The information on the dynamics also is lost when the decay rates Γ_N , and Γ_{nN} are normalized to Γ_{NM} . This normalization is the usual procedure; see for instance [36, Eq. (7)], and [49, Eqs. (14),(15)]. With this normalization, the spectra depend on the phase space and the FSIs, but very weakly on the NMWD dynamics. The same happens when the transition density is normalized to the decay rate (See [57, Fig. 3].) In contrast, as explained below, we do not normalize any of the calculated transition rates, and this allows us to inquire more deeply into the NMWD mechanism.^c

The measurement implies the counting of the numbers of emitted protons ΔN_p^i and the errors $\delta\Delta N_p^i$, corrected by the detection efficiency, within m energy bins of width ΔE . The total number of emitted protons and the resulting errors are

$$N_p = \sum_{i=1}^m \Delta N_p^i, \quad \delta N_p = \sqrt{\sum_{i=1}^m (\delta\Delta N_p^i)^2}, \quad (5)$$

where the summation goes over proton energies E_p^i larger than a given threshold energy E_{thres} .

^cIt might be useful to draw a parallel with electromagnetic decay. When the electric $E2$ and the magnetic $M1$ multipoles are the lowest allowed transitions, both may contribute significantly to the total rate $\Gamma_\gamma = \Gamma_\gamma(E2) + \Gamma_\gamma(M1)$, since the electric transition may be enhanced substantially above the single particle estimate due to collective effects. The comparison between theory and data is always done for the decay rates $\Gamma_\gamma(E2)$ and $\Gamma_\gamma(M1)$, separately. There is no physical motivation for comparing the ratios $\Gamma_\gamma(E2)/\Gamma_\gamma$ and $\Gamma_\gamma(M1)/\Gamma_\gamma$, since they are less sensitive to the nuclear structure effects than the individual decay rates.

The corresponding total decay rate with its error read

$$\Gamma_p = \sum_{i=1}^m \Delta\Gamma_p^i, \quad \delta\Gamma_p = \sqrt{\sum_{i=1}^m (\delta\Delta\Gamma_p^i)^2}, \quad (6)$$

where, as seen from (4), the decay rates $\Delta\Gamma_p^i(E_p)$ with errors $\delta\Delta\Gamma_p^i$ are given by

$$\Delta\Gamma_p^i(E_p) = \frac{\Gamma_W}{N_W} \Delta N_p^i(E_p), \quad (7)$$

and

$$\delta\Delta\Gamma_p^i = \frac{\Gamma_W}{N_W} \Delta N^i \left[\left(\frac{\delta\Delta N^i}{\Delta N^i} \right)^2 + \left(\frac{\delta\Gamma_W}{\Gamma_W} \right)^2 + \left(\frac{\delta N_W}{N_W} \right)^2 \right]^{1/2}, \quad (8)$$

with $\delta\Gamma_W$, and δN_W being, respectively, the experimental errors on Γ_W , and N_W . Thus, to evaluate the experimental decay rates we need to know the values of Γ_W and N_W for each hypernucleus. As usually done all Γ 's will be given in units of Γ_Λ , the total decay width of the free Λ .

For the first quantity we can use the relationship

$$\Gamma_W(A) = (0.990 \pm 0.094) + (0.018 \pm 0.010) A, \quad (9)$$

which was derived in Ref.²³ from a linear fit to the known values of all measured hypernuclei in the mass range $A = 4 - 12$.

But unfortunately there is no experimental information about N_W in the literature. Only the ratio

$$R_p = \frac{N_p}{N_W}, \quad (10)$$

for the eight hypernuclei discussed here were presented at a conference,⁵⁰ for the threshold energy $E_{thres} = 15$ MeV. We will use, however, only the results for ${}^5_\Lambda\text{He}$, ${}^7_\Lambda\text{Li}$, and ${}^{12}_\Lambda\text{C}$, since only these were published in a refereed physics journal so far.²² We list them in Table 1, together with values of N_p from Ref.,²⁴ and the resulting estimates for N_W from (10). The proton decay rates, evaluated from

$$\Gamma_p = R_p \Gamma_W, \quad (11)$$

are also shown. Since, according to (9), the value of Γ_W is close to unity, the last result implies that the ratio R_p is basically the proton decay rate.

The theoretical analogs of (6) and (7) are, respectively

$$\Gamma_p^{th} = \int S_p(E_p) dE_p, \quad (12)$$

and

$$\Delta\Gamma_p^{th}(E_p) = S_p(E_p) \Delta E, \quad (13)$$

where the spectral function $S_p(E_p)$ depends on the theory that is used to evaluate the NMWD, which not yet has been discussed.

Table 1. Values of R_p from Ref.²² and N_p from Ref.²⁴ for $E_{thres} = 15$ MeV, together with the resulting estimates for N_W , and $\Gamma_p = R_p\Gamma_W$.

Hypernucleus	R_p	N_p	N_W	Γ_p
${}^5_{\Lambda}\text{He}$	0.25 ± 0.07	262 ± 25	1047 ± 391	0.27 ± 0.11
${}^7_{\Lambda}\text{Li}$	0.37 ± 0.09	259 ± 21	700 ± 226	0.41 ± 0.16
${}^{12}_{\Lambda}\text{C}$	0.43 ± 0.07	678 ± 38	1576 ± 344	0.52 ± 0.18

Instead of comparing the experimental transition rates with the calculated rates, we can compare directly the number of measured protons with the calculated quantity

$$\Delta N_p^{th}(E_p) = \frac{N_W}{\Gamma_W} S(E_p) \Delta E, \quad (14)$$

where N_W/Γ_W is just a proportionality factor.

All the above is completely general. The theory that is used can be as complicated as necessary to properly interpret experimental data. But it can also be very simple and still lead us to correct conclusions about the underlying physics.^d Such a model is described below.

3. Independent Particle Shell Model for the Spectral Function

The IPSM has been used for more than twenty years in the evaluation of the $1N$ -NM decay rates,^{51,52} but only in recent years was it applied for the description of different spectral densities $S_N(E)$, $S_{nN}(E)$, $S_{nN}(\cos\theta)$, and $S_{nN}(P)$.^{8-10,43,44,53-59} We briefly sketch here the main assumptions that are made in this model, and give the resulting theoretical expression for the proton kinetic energy spectrum.

The assumptions are: (i) the initial hypernuclear state is taken as a hyperon Λ in a single-particle state $j_\Lambda = 1s_{1/2}$ weakly coupled to an $(A-1)$ nuclear core of spin J_C , i.e., $|J_I\rangle \equiv |(J_C j_\Lambda) J_I\rangle$; (ii) the nucleon ($N = p, n$) inducing the decay is in the single-particle state j_N ($j \equiv nlj$); (iii) the final residual nuclear states are: $|J_F\rangle \equiv |(J_C j_N^{-1}) J_F\rangle$; (iv) the liberated energy is

$$\Delta_N^j = \Delta + \varepsilon_\Lambda + \varepsilon_N^j, \quad (15)$$

where $\Delta = M_\Lambda - M_p = 177.33$ MeV, and the ε 's are experimental single-particle

^dThe model used to describe a process should, in principle, describe all the involved physics. This is a desirable condition, but it is not in any way essential. Useful models are those that allow us to infer consequences consistent with the observations. More precisely, a model is a simplified version of the process, and the model designer decides which features to consider.

energies (s.p.e.)^e, and (v) the c.m. momenta and relative momenta of the emitted particles are:

$$P_{nN} = \sqrt{(A-2)(2M\Delta_N^j - p_n^2 - p_N^2)},$$

$$p_{nN} = \sqrt{M\Delta_N^j - \frac{A}{4(A-2)}P_{nN}^2}.$$

It follows that the $1N$ -NM decay rate is given by⁵⁹

$$\Gamma_N = \sum_j \Gamma_N^j; \quad \Gamma_N^j = \int \mathcal{I}_N^j(p_{nN}, P_{nN}) d\Omega_{nN},$$

where $d\Omega_{nN}$ is the phase space factor, and

$$\mathcal{I}_N^j(p, P) = \frac{1 + \delta_{Nn}}{2} \sum_{J=|j-1/2|}^{J=j+1/2} F_{NJ}^j \sum_{SILT} |\mathcal{M}(plPL\lambda SJT; j_\Lambda j_N JT)|^2,$$

with

$$\begin{aligned} \mathcal{M}(plPL\lambda SJT; j_\Lambda j_N JT) &= \frac{1}{\sqrt{2}} [1 - (-)^{l+S+T}] \\ &\times \mathcal{O}_L(P)(lL\lambda SJT|V(p)|j_\Lambda j_N JT), \end{aligned}$$

and

$$\mathcal{O}_L(P) = \int R^2 dR j_L(PR) R_{0L}(b/\sqrt{2}, R).$$

Here L , l , and λ are, respectively, the c.m., relative, and total orbital angular momenta ($\boldsymbol{\lambda} = \mathbf{L} + \mathbf{l}$), while V is the transition potential, and b is the harmonic oscillator length parameter.

The kinematics of different spectra S_N depend on $d\Omega_{nN}$ and on the overlap $\mathcal{O}_L(P_{nN})$, while the decay dynamics is contained in the matrix element $(lL\lambda SJT|V(p_{nN})|j_\Lambda j_N JT)$. The information on nuclear structure is enclosed in the spectroscopic factors F_{NJ}^j , which account for the Pauli Principle within each single-particle shell j_N . In the general case, they are given by

$$F_{NJ}^j = (2J+1) \sum_{J_F^n} \left\{ \begin{matrix} J_C & J_I & j_\Lambda \\ J & j_N & J_F \end{matrix} \right\}^2 |\langle J_C || a_{j_N}^\dagger || J_F^n \rangle|^2, \quad (16)$$

where $\langle J_C || a_{j_N}^\dagger || J_F^n \rangle$ are the fractional parentage coefficients (FPCs), and the summation goes over the n final states J_F^n in the residual $(A-2)$ nuclei, with the same

^eThe schematically drawn energies in [59, Fig. 7] are the experimental s.p.e., which can be identified with the SM s.p.e. only in closed shell nuclei, such as ^{16}O . For open shell nuclei, which is the case of ^{12}C , the experimental s.p.e. are frequently identified with the quasiparticle energies, which include the effect of pairing correlations, and could be quite different from the SM s.p.e.. This was done, for instance, in [60, Table IV], where the experimental and SM s.p.e. are listed, respectively, in columns two and five. Moreover, the correct $p_{3/2}$, $p_{1/2}$ and $d_{5/2}$ experimental energies read, respectively, -15.96 , -1.95 , and 1.61 MeV.⁶²

spin, parity, and isospin, and different excitation energies. Such a detailed description could be redundant since, in the NMWD, we evaluate the inclusive decay rate, without being interested in exclusive processes that feed each of the individual final states J_F^n . Thus, within the IPSM, the spectroscopic factor becomes much simpler since $|J_F^n\rangle \rightarrow |(J_C j_N^{-1})J_F\rangle$, and the summation goes only over the values of J_F that fulfill the constraint $|J_C - j_N| \leq J_F \leq J_C + j_N$. The values for J_I and J_C are taken from experimental data and, for the hypernuclei of interest here, are listed in Table I of Ref.⁵⁹ The resulting factors F_{NJ}^j are listed in Table II of the same paper.

The spectra are obtained from the differentiation of Γ_N with respect to E_N , $\cos \theta_{nN}$, E_{nN} , and P_{nN} . In particular, for the kinetic energy spectrum, one has:

$$S_N(E_N) = \sum_j S_N^j(E_N), \quad (17)$$

with

$$S_N^j(E_N) = (A-2) \frac{8M^3}{\pi} \int_{-1}^{+1} d \cos \theta_{nN} \sqrt{\frac{E_N}{E'_N}} E_n \mathcal{I}_{j_N}(pP),$$

where

$$E'_N = (A-2)(A-1)\Delta_N^j - E_N[(A-1)^2 - \cos^2 \theta_{nN}],$$

and

$$E_n = \left[\sqrt{E'_N} - \sqrt{E_N} \cos \theta_{nN} \right]^2 (A-1)^{-2}.$$

Finally,

$$\Gamma_N \equiv \sum_j \Gamma_N^j = \sum_j \int_0^{Q_N^j} S_N^j(E_N) dE_N, \quad Q_N^j = \frac{A-2}{A-1} \Delta_N^j, \quad (18)$$

with Q_N^j being the single-particle Q-values.

The outline of the numerical calculation is the following:

- (1) The transition potential $V(p_{nN})$ for the emission of the nN pair, contained in $\mathcal{T}_{NJL}^j(p_{nN})$, is described by three OME models, namely: P1 - The full pseudoscalar (π, K, η) and vector (ρ, ω, K^*) meson octets (PSVE), with the weak coupling constants, and dipole form-factor cutoffs Λ_M from Refs.;^{3,4,11} P2 - Only one- $(\pi + K)$ exchanges (PKE) are considered, with the same parametrization as in the previous case, *i.e.*, with cutoffs $\Lambda_\pi = 1.3$ GeV and $\Lambda_K = 1.2$ GeV from;⁴ and P3 - The soft $\pi + K$ exchange (SPKE) potential with cutoffs $\Lambda_\pi = 0.7$ GeV and $\Lambda_K = 0.9$ GeV from.^{8,9}
- (2) The SRCs acting on final nN states are incorporated phenomenologically through Jastrow-like SRC functions, as used within both finite nuclei calculations,^{4,53-56} and Fermi Gas Model (FGM) calculations.^{25,61}

4. Proton Decay Rates and FINUDA data

The calculated transition densities $\Delta\Gamma_p^{th}(E_p)$, for $\Delta E = 10$ MeV and evaluated from (13) with $S_p(E_p)$ given by (17) are shown in Fig. 2 for the hypernuclei measured by FINUDA.²⁴ As expected, in all cases the spectra strongly depend on the parameterization that is used for the transition potential, while their shapes are the same for all practical purposes. The experimental values of $\Delta\Gamma_p(E_p)$ for ${}^5_{\Lambda}\text{He}$, ${}^7_{\Lambda}\text{Li}$, and ${}^{12}_{\Lambda}\text{C}$, evaluated from (7) for the values of $\Delta N_p(E_p)$ shown in [24, Fig. 1], are also displayed in the same figure. Their errors were calculated from (8).

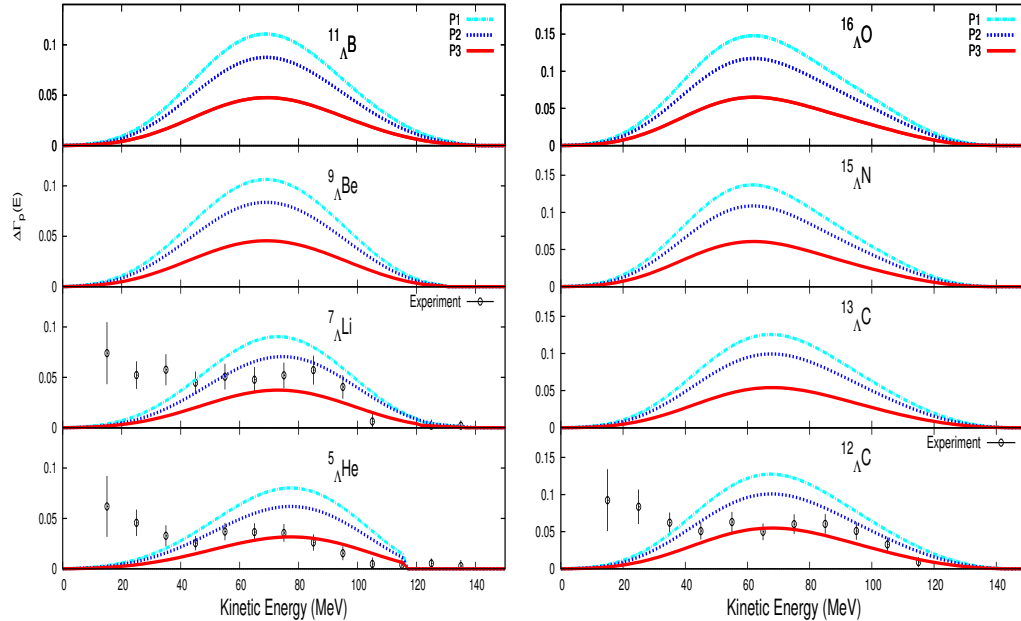


Fig. 2. (Color online) Calculated proton kinetic energy spectra $\Delta\Gamma_p^{th}(E_p)$ for three different transition potentials specified in the previous section. For ${}^5_{\Lambda}\text{He}$, ${}^7_{\Lambda}\text{Li}$, and ${}^{12}_{\Lambda}\text{C}$ are also shown the values of $\Delta\Gamma_p(E_p)$ evaluated from (7) that correspond to the $\Delta N_p(E_p)$ shown in [24, Fig. 1].

With the parametrization P1, the theory greatly overestimates the experimental spectra at medium and high energies ($E_p \gtrsim 40$ MeV), underestimating them at low energies. The discrepancy can not be settled by simply opening a new $2N$ -NM decay channel induced by two nucleons, since this decay mode, although capable of producing additional particles at low energies, is unable to lower the transition strength at high energies. Nor is it possible for the FSIs to solve the problem, since they can hardly change the total transition density induced by a proton. They can only remove a portion of the strength from high energy to low energy. It is self-evident from Fig. 2 that such a mechanism cannot be successful in the present case.

Improved agreement is obtained in the P2 model, which means that the incor-

poration of vector mesons, instead of improving the agreement, makes it poorer. However, the high energy part of the ${}^5_{\Lambda}\text{He}$ spectrum is reproduced fairly well only with the parametrization P3. The decrease in magnitude of proton spectra in going from P1 to P2 is due to the well known fact that the parity-violating contribution of the vector mesons to the proton transition rates is quite sizable (see, for instance, [53, Table IV]). On the other hand, the strong variation of the same observable in ${}^5_{\Lambda}\text{He}$ with regard to the BBM vertex functions is thoroughly discussed in [8, Fig. 1].

Table 2. Transition rates Γ_p^{th} calculated from (12) for all three parametrizations and with two different threshold energies: $E_{thres} = 15$ MeV, and $E_{thres} = 40$ MeV. For ${}^5_{\Lambda}\text{He}$, ${}^7_{\Lambda}\text{Li}$, and ${}^{12}_{\Lambda}\text{C}$ the values of Γ_p and their errors, evaluated from (6), are also shown.

Hypernucleus	Γ_p	Γ_p^{P1}	Γ_p^{P2}	Γ_p^{P3}
<u>$E_{thres} = 15$ MeV</u>				
${}^5_{\Lambda}\text{He}$	0.27 ± 0.05	0.466	0.360	0.185
${}^7_{\Lambda}\text{Li}$	0.41 ± 0.07	0.531	0.415	0.228
${}^9_{\Lambda}\text{Be}$		0.627	0.494	0.275
${}^{11}_{\Lambda}\text{B}$		0.667	0.527	0.289
${}^{12}_{\Lambda}\text{C}$	0.52 ± 0.07	0.792	0.627	0.343
${}^{13}_{\Lambda}\text{C}$		0.776	0.614	0.336
${}^{15}_{\Lambda}\text{N}$		0.821	0.651	0.365
${}^{16}_{\Lambda}\text{O}$		0.906	0.718	0.399
<u>$E_{thres} = 40$ MeV</u>				
${}^5_{\Lambda}\text{He}$	0.19 ± 0.04	0.428	0.331	0.171
${}^7_{\Lambda}\text{Li}$	0.27 ± 0.05	0.488	0.381	0.204
${}^9_{\Lambda}\text{Be}$		0.555	0.437	0.243
${}^{11}_{\Lambda}\text{B}$		0.607	0.481	0.263
${}^{12}_{\Lambda}\text{C}$	0.37 ± 0.06	0.719	0.569	0.311
${}^{13}_{\Lambda}\text{C}$		0.706	0.559	0.305
${}^{15}_{\Lambda}\text{N}$		0.721	0.573	0.320
${}^{16}_{\Lambda}\text{O}$		0.801	0.635	0.352

At this stage, it might be useful to recall that, in all theoretical descriptions of the NMWD, only three body final states have been considered, implying that the residual nuclei are necessarily bound. Obviously, this is done for simplicity, but does not always occur. The most emblematic case is that of ${}^{11}_{\Lambda}\text{B}$, which has been considered in many theoretical studies done so far. However, its parent nucleus in the neutron channel, ${}^{11}\text{B}$, is unstable and disintegrates into $p+2\alpha$ with a half-life of $8 \cdot 10^{-19}$ s, which is very short when compared with the half-life of ${}^{11}_{\Lambda}\text{B}$. Among the

nonmesonic decays analysed here, the same occurs with the ${}^5\text{He}$ nucleus, which is the residual nucleus for the proton NMWD of ${}^7_\Lambda\text{Li}$. In fact, it is unstable to particle emission, decaying into $p + {}^4\text{He}$ with a half life of $70(3) \cdot 10^{-25} \text{s}$. This time is much shorter than the lifetime of ${}^7_\Lambda\text{Li}$ and, therefore, the instability of ${}^5\text{He}$ could be the cause of the discrepancy between theory and experiment at high energy.

Table 3. Spectroscopic factors and the transition rates Γ_p for ${}^7_\Lambda\text{Li}$ evaluated in the intermediate coupling model with the wave function amplitudes a_{LS} given in Ref.,⁶³ which are also listed.

a_{LS}					
LS	<i>fit69</i>	<i>fit5</i>	<i>CK616</i>	<i>CK616</i>	CKPOT
01	0.9873	0.9906	0.9576	0.9484	0.9847
12	-0.0422	-0.0437	-0.2777	-0.3093	-0.1600
10	-0.1532	-0.1298	-0.0761	-0.0703	-0.0685
F_{NJ}^j					
J, lj					
0, $p_{1/2}$	0.0320	0.0311	0.0693	0.0790	0.0419
1, $p_{1/2}$	0.3023	0.3032	0.3026	0.3022	0.3042
1, $p_{3/2}$	0.5255	0.5259	0.4973	0.4903	0.5175
2, $p_{3/2}$	0.1403	0.1399	0.1307	0.1286	0.1364
Γ_p	0.2444	0.2444	0.2475	0.2483	0.2453

Similarly to what was done in Figure 2 for proton kinetic energy spectra $\Delta\Gamma_p^{th}(E_p)$, the theoretical results for the proton decay rates (18) for two different threshold energies ($E_{thres} = 15 \text{ MeV}$, and $E_{thres} = 40 \text{ MeV}$) are shown in Table 2. For ${}^5_\Lambda\text{He}$, ${}^7_\Lambda\text{Li}$, and ${}^{12}_\Lambda\text{C}$ the experimental values of Γ_p and their errors, evaluated from (6), are also shown.

All that was previously stated when comparing the theory with the data in Figure 2 also applies here. In particular, since the theory does not include the 2N-NM channel, the experimental transition rates must always be larger than the theoretical rates for $E_{thres} = 15 \text{ MeV}$. This condition is satisfied only for the parameterization P3, suggesting that the other two sets of parameters would not be appropriate. On the other hand, as the FSIs, which remove the density transition from the high energy region, are omitted in the calculations, all three Γ_p^{th} should be larger than Γ_p for $E_{thres} = 40 \text{ MeV}$. From Table 2, we see that within the experimental errors this is indeed the case. However, in calculations P2 and P3, the differences between the data and the theory are too large to be entirely attributed to the lack of the FSIs in the theory.

It would also be interesting to compare the experimental results shown in the

upper part of Table 2 with the calculation done by Itonaga and Motoba¹⁷ with a more elaborate SM than that used here, employing the $\pi + 2\pi/\rho + 2\pi/\sigma + \omega + K + \rho\pi/a_1 + \sigma\pi/a_1$ exchange potential. They obtain: $\Gamma_p^0({}^5_\Lambda\text{He}) = 0.237$, and $\Gamma_p^0({}^{12}_\Lambda\text{C}) = 0.534$. In the first case, Γ_p is greater than Γ_p^0 as it should be, but it is lower in the second case which is not correct.

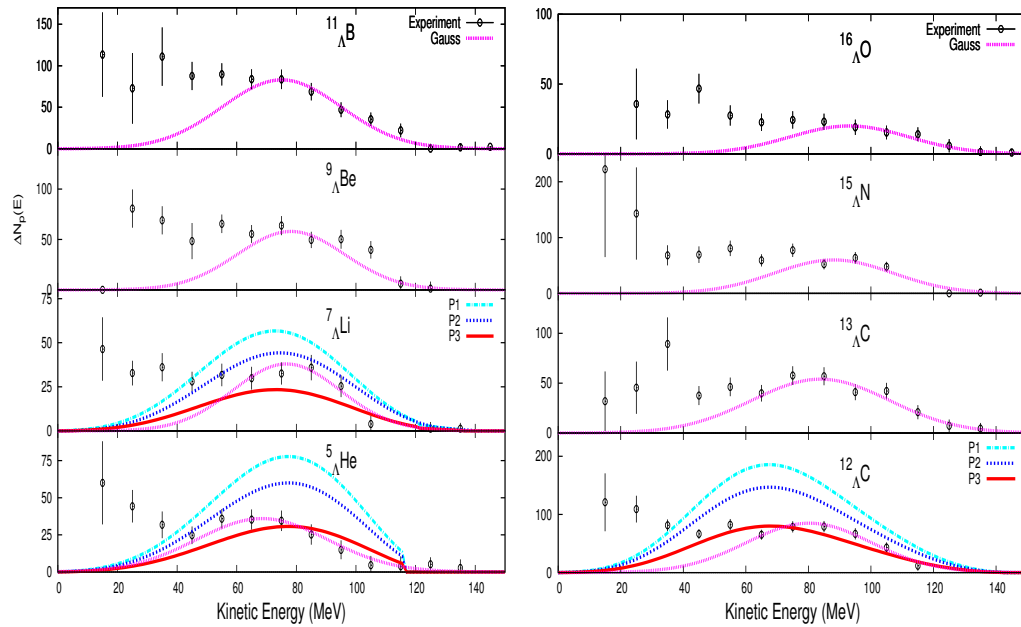


Fig. 3. (Color online) Experimental data²⁴ for proton kinetic energy spectra for the number of particles $\Delta N_p(E_p)$ are compared with the IPSM results for three different OME potentials. Theoretical results have been evaluated from equation (14). Also shown are the Gaussian-function fits of each proton spectrum from 80 MeV onwards, performed in Ref.²⁴

It can be argued that a derivation of the $F_{N,J}^j$, based on the jj single-particle model, is not fully appropriate for light nuclei, such as Li and Be, with the intermediate coupling model preferred over pure jj coupling for the core nuclei. In fact, the structure of these nuclei is closer to LS coupling than to an assembly of $p_{3/2}$ valence nucleons, as can be seen, for instance, from [63, Table 5] where the core state $J_C = 1^+$ in ${}^7_\Lambda\text{Li}$ is basically a pure 3S state. In this case, instead of the spectroscopic factors $F_{N1}^{p_{3/2}} = 5/8$, and $F_{N2}^{p_{3/2}} = 5/8$ given in Ref. [59, Table 2], one has $F_{N1}^{p_{3/2}} = 19/36$, $F_{N2}^{p_{3/2}} = 5/36$, $F_{N0}^{p_{1/2}} = 1/36$, and $F_{N1}^{p_{1/2}} = 11/36$. Within the parametrization P3, the last spectroscopic factors yield $\Gamma_p = 0.244$ which is only slightly larger than the value 0.228 shown in Table 1. However, to justify even more reliably the jj coupling, we have recalculated Γ_p with five different wave functions evaluated in the intermediate-coupling model, and cited in.⁶³ Their amplitudes a_{LS}

are listed in Table 3. The spectroscopic factors (6) are evaluated from the expression

$$F_{pJ}^j = 3(2J+1)(2j_p+1) \sum_{J_F=1/2,3/2} (2J_F+1) \left\{ \begin{matrix} 1 & \frac{1}{2} & \frac{1}{2} \\ J & j_p & J_F \end{matrix} \right\}^2 \times \sum_{LS} (2L+1)(2S+1) \left[a_{LS} \left\{ \begin{matrix} 1 & \frac{1}{2} & j_p \\ 1 & \frac{1}{2} & J_F \\ L & S & 1 \end{matrix} \right\} \right]^2. \quad (19)$$

The results are shown in Table 3, from which it can be concluded that the difference between the jj coupling and the intermediate coupling is $\leq 10\%$. The physical reason for this fact is that Γ_p is an inclusive quantity, so it is not acutely relevant if the proton decays from orbital $p_{3/2}$ or $p_{1/2}$.

We would like to stress that the way to compare the theory with data as done here, as well as in a previous paper,^{9,44} is conceptually different from the traditional way.^{4,16,17,36,38,49,64} This can be seen immediately by confronting expression (13) with [36, Eq. (7)]. Instead of comparing different bare proton contributions Γ_p^0 , Γ_n^0 , Γ_2^0, \dots , which are not directly measured but are extracted by the experimentalist from the data, we compare the total decay rate Γ_p and the corresponding spectra, which include all of the protons that come from the NMWD. Different extraction procedures are not unambiguous, as we have discussed in the first version of the present work⁶⁵ regarding the derivation of Γ_2^0 by both KEK,²¹ and FINUDA.²⁴ More details on the second extraction procedure are given in the next section.

Fig. 3 is just the replica of Fig. 2 except for the numbers of protons, with $\Delta N_p^{th}(E_p)$ evaluated from (14). For reasons of completeness, in the last figure we show the spectra of all measured hypernuclei. Obviously, the two figures lead to the same conclusions. The Gaussian-function fits of each proton spectrum from 80 MeV onwards, that were performed in Ref.²⁴ and that will be discussed in the next section, are displayed also in the last figure.

5. Extraction of branching ratio Γ_2^0/Γ_{NM}^0 from the data

The determination of the branching ratio Γ_2^0/Γ_{NM}^0 by FINUDA²⁴ is based on the partition of the total number of detected protons N_p into low, and high energy regions populated, respectively, by $N_p^< \equiv N_p(E_p < E_{part})$, and $N_p^> \equiv N_p(E_p > E_{part})$ protons relative to the partition energy E_{part} . After assuming that all 2N-NM protons are contained within $N_p^<$, they define the ratio

$$R \equiv \frac{N_p^<}{N_p} = \frac{N_p^{0<} + N_2^0 + N_{FSI}^<}{N_p^0 + N_2^0 + N_{FSI}} = \frac{\Gamma_p^{0<}/\Gamma_p^0 + \Gamma_2^0/\Gamma_p^0 + N_{FSI}^</N_p^0}{1 + \Gamma_2^0/\Gamma_p^0 + N_{FSI}/N_p^0}, \quad (20)$$

where N_p^0 and N_2^0 are, respectively, the numbers of protons induced by the 1N-NM, and 2N-NM decays, and $N_{FSI} = N_{FSI}^< + N_{FSI}^>$ is the total number of particles produced by the FSIs.

The next steps done in Ref.²⁴ are not supported by sufficiently firm physical arguments. Namely, it is assumed: i) that the proton spectra from 80 MeV onwards

are due entirely to protons coming from the $\Lambda p \rightarrow np$ reaction, ii) that they can be fit by Gaussian curves shown in Fig. 3, and iii) that the maxima of these curves correspond to the partition energies E_{part} . All of this yields

$$R \equiv \frac{N_p^<}{N_p} = \frac{0.5 + \Gamma_2^0/\Gamma_p^0 + N_{FSI}^</N_p^0}{1 + \Gamma_2^0/\Gamma_p^0 + N_{FSI}^</N_p^0}, \quad (21)$$

since the Gaussian curves are bell shaped, satisfying always the condition $\Gamma_p^{0<} \equiv \Gamma_p^0(E_p < E_{\text{max}}) = \Gamma_p^{0>} \equiv \Gamma_p^0(E_p > E_{\text{max}})$. The resulting partition energies $E_{\text{max}}^{\text{FINUDA}}$ are listed in the second column of Table 4.

Table 4. Mean values of FINUDA Gaussian fits²⁴(in units of MeV) are confronted with the maxima of proton spectra with the theoretical maxima (third column), as well as with the energies $E_{\text{even}}^{\text{th}}$ for which the proton strength is evenly distributed, *i.e.*, $\Gamma_p^{0>} \equiv \Gamma_p^{0<}$ (fourth column).

Hypernucleus	$E_{\text{max}}^{\text{FINUDA}}$	$E_{\text{max}}^{\text{th}}$	$E_{\text{even}}^{\text{th}}$
${}^5_{\Lambda}\text{He}$	68.5 ± 4.1	77.5	75.0
${}^7_{\Lambda}\text{Li}$	76.7 ± 5.2	73.5	72.0
${}^9_{\Lambda}\text{Be}$	78.2 ± 6.2	69.0	69.0
${}^{11}_{\Lambda}\text{B}$	75.1 ± 5.0	69.0	70.5
${}^{12}_{\Lambda}\text{C}$	80.2 ± 2.1	67.5	70.5
${}^{13}_{\Lambda}\text{C}$	83.9 ± 12.8	67.5	70.5
${}^{15}_{\Lambda}\text{N}$	88.1 ± 6.2	61.5	66.0
${}^{16}_{\Lambda}\text{O}$	93.1 ± 6.2	61.5	66.0

Next, FINUDA approximated (21) by a linear function of the mass number A , *i.e.*,

$$R(A) = a + bA, \quad (22)$$

where

$$a = \frac{0.5 + \Gamma_2^0/\Gamma_p^0}{1 + \Gamma_2^0/\Gamma_p^0}, \quad (23)$$

does not depend on A . Finally, a χ^2 fit for $R(A)$ was done for the energies $E_{\text{max}}^{\text{FINUDA}}$ to obtain the values of a and b that are shown in row A of Table 5, together with the resulting Γ_2^0/Γ_p^0 , and Γ_2^0/Γ_{NM}^0 derived from

$$\frac{\Gamma_2^0}{\Gamma_p^0} = \frac{a - 0.5}{1 - a}, \quad \frac{\Gamma_2^0}{\Gamma_{NM}^0} = \frac{a - 0.5}{(1 - a)\Gamma_n^0/\Gamma_p^0 + 0.5}, \quad (24)$$

for the experimental value $\Gamma_n^0/\Gamma_p^0 = 0.48 \pm 0.08$, measured by KEK.³⁵

The FINUDA procedure to extract the value of Γ_2^0 from a series of kinetic energy spectra, by separating them into low and high energy regions, looks physically sound. However, we shall soon see that it is very sensitive to the separation procedure. On the other hand, in the fitting of the spectra with Gaussian curves, FINUDA implicitly assumes the absence of $N_{FSI}^>$, which is not only unrealistic, but also not necessary.

Before separating the spectra, we compare the calculated energy locations E_{\max}^{th} of the spectra maxima with the maxima of the FINUDA Gaussian fits E_{\max}^{FINUDA} . From Figs. 2 and 3, one immediately notices sizeable differences. Moreover, from Table 4, one sees that, while the maxima E_{\max}^{FINUDA} increase from 68.5 MeV to 93.1 MeV in going from ${}^5_{\Lambda}\text{He}$ to ${}^{16}_{\Lambda}\text{O}$, the energies E_{\max}^{th} decrease from 77.6 MeV to 61.5 MeV. On the other hand, while the Gaussian curves are bell shaped, the theoretical 1N-NM spectra deviate significantly from a symmetrical shape. More precisely, the calculated $\Gamma_p^{0<}$ is greater than $\Gamma_p^{0>}$ in ${}^5_{\Lambda}\text{He}$, ${}^7_{\Lambda}\text{Li}$, and ${}^9_{\Lambda}\text{Be}$, and smaller for the remaining hypernuclei.

The reason for this can be understood from an inspection of Fig. 4, where the spectra of ${}^5_{\Lambda}\text{He}$ and ${}^{16}_{\Lambda}\text{O}$ without recoil (a) and with recoil (b) are displayed. First, as expected, the recoil effect is sizeable in ${}^5_{\Lambda}\text{He}$ where only the orbital $s_{1/2}$ contributes. Second, the ${}^5_{\Lambda}\text{He}$ spectrum does not have the symmetric bell shape, mainly because the single kinetic energy reaches its maximum value rather abruptly at ~ 115 MeV due to the recoil factor $(A-2)/(A-1) = 3/4$ in Eq. (18) for $Q_p^{s_{1/2}}$; this effect, however, does not modify the value of $E_{\max} = 77.6$ MeV, but causes $\Gamma_p^{0<}$ to be appreciably larger than $\Gamma_p^{0>}$ ($\Gamma_p^{0<} \cong 0.55 \Gamma_p^{0>}$). Third, in the case of ${}^{16}_{\Lambda}\text{O}$, three partial waves ($s_{1/2}$, $p_{3/2}$, and $p_{1/2}$) contribute with different heights and widths, the convolution of which is a nonsymmetric proton spectrum with $\Gamma_p^{0<} = 0.43 \Gamma_p^{0>}$; here the energy E_{\max} becomes significantly smaller because the energy $\Delta_p^{s_{1/2}}$, given by (15), is ~ 25 MeV smaller in ${}^{16}_{\Lambda}\text{O}$ than in ${}^5_{\Lambda}\text{He}$. Briefly, as the value of A increases, the average value of the binding energies ε_{Λ} and ε_N^j turns out to be larger (see Ref. [66, Fig. 11]), which makes the energy position of the maximum E_{\max}^{th} for the 1N-NM proton kinetic energy spectrum become increasingly smaller. The numerical results for E_{\max}^{th} are shown in Table 4, where they are compared with the peaks of the FINUDA Gaussian fits E_{\max}^{FINUDA} .²⁴ Note that E_{\max}^{th} decreases with the mass number while E_{\max}^{FINUDA} increases. Thus, they differ from one another quite significantly and the difference increases from 9 MeV in ${}^5_{\Lambda}\text{He}$ up to 32 MeV in ${}^{16}_{\Lambda}\text{O}$.

The energies E_{\max} are closely related to the liberated energies, *i.e.*, to the Q_p^j -values since the latter should, in principle, also decrease when the Δ_p^j decrease. However, for light hypernuclei, this decrease is largely offset by the recoil effect, as shown by Eq. (18). The final results, displayed in Figs. 2 and 3, demonstrate that the Q-values are roughly constant and within the energy interval of $\sim 115 - 135$ MeV, which is consistent with the data within experimental errors.^f

^f One should also mention that it is assumed here that the residual nucleus is emitted in the ground state, and that consideration of excitation energies could further diminish the Q-values.

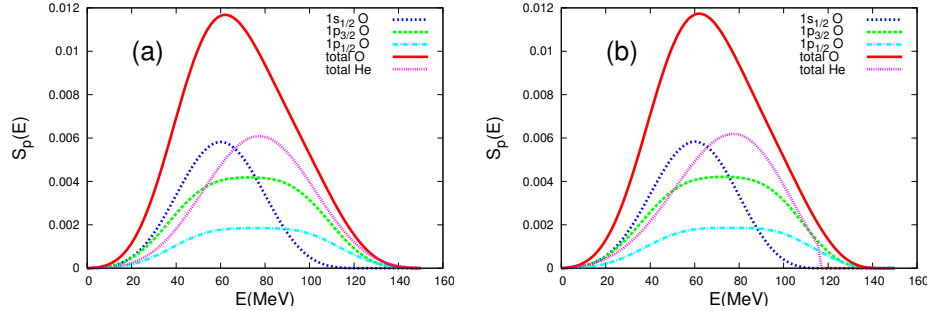


Fig. 4. (Color online) ${}^5_{\Lambda}\text{He}$ and ${}^{16}_{\Lambda}\text{O}$ spectra: (a) without recoil, and (b) with recoil, evaluated within the IPISM for the P2 OME transition potential. Contributions of different orbitals $s_{1/2}$, $p_{3/2}$, and $p_{1/2}$ to the total ${}^{16}_{\Lambda}\text{O}$ spectra are also displayed.

Table 5. Results for the χ^2 parameters a and b , and the corresponding ratios Γ_2^0/Γ_p^0 , and $\Gamma_2^0/\Gamma_{\text{NM}}^0$ for FINUDA data,²⁴ and different partition energies for $N_p^<$, and $N_p^>$: A) derived in Ref.²⁴ with $E_{\text{max}}^{\text{FINUDA}}$, B) and C) obtained here with $E_{\text{max}}^{\text{th}}$, and $E_{\text{even}}^{\text{th}}$, respectively.

case	a	b	Γ_2^0/Γ_p^0	$\Gamma_2^0/\Gamma_{\text{NM}}^0$
A	0.654 ± 0.138	0.009 ± 0.013	0.43 ± 0.25	0.24 ± 0.10
B	0.711 ± 0.101	-0.010 ± 0.008	0.73 ± 0.61	0.33 ± 0.10
C	0.656 ± 0.101	-0.004 ± 0.008	0.45 ± 0.43	0.23 ± 0.09

In view of the differences between the FINUDA spectra and those calculated here, one is immediately tempted to repeat the above analysis using the energies $E_{\text{max}}^{\text{th}}$ instead of $E_{\text{max}}^{\text{FINUDA}}$. This was done and the results for R are shown in the left panel of Figure 5, along with the corresponding linear χ^2 fit. The large difference between the two sets of maxima gives rise to large differences between the values of the ratios R in Ref. [24, Fig. 2] and those derived here. The parameters a and b , and the ratios Γ_2^0/Γ_p^0 , and $\Gamma_2^0/\Gamma_{\text{NM}}^0$ obtained in this way are listed in row B of Table 5. The value of a is not very different from the previous case but, as expected, b is now negative, and the resulting Γ_2^0 is significantly different due to its strong sensitivity on a in (24).

One must not forget here that, while the number of protons can be partitioned in many different ways, obtaining different results for the ratio defined in (20), the relations from (21) on are only valid when the condition $\Gamma_p^{0<} = \Gamma_p^{0>} = \Gamma_p^0/2$

After finishing this work, we learned that Bufalino,⁶⁷ one of the coauthors of Ref. ²⁴ has proposed evaluating partition energies as half the Q-values in the 150 – 166 MeV range. In this way, she obtains good agreement with $E_{\text{max}}^{\text{FINUDA}}$ for A from 5 to 9, whereas for $A = 13, 15$, and 16 there is a 2σ discrepancy. Note that the last range for the Q-values implies unrealistically small proton separation energies.

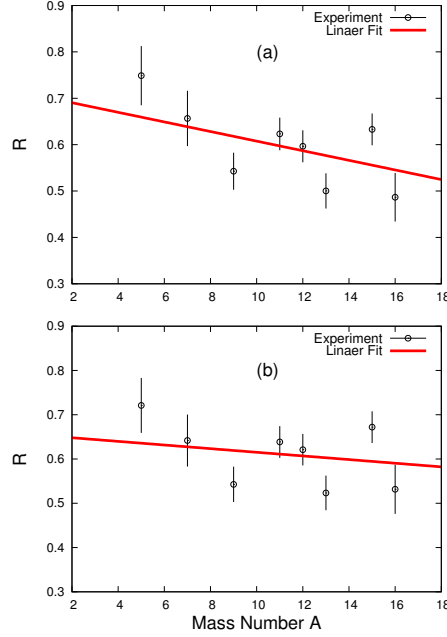


Fig. 5. (Color online) Ratio R , given by (11) as a function of A for the partition energies: (a) E_{\max}^{th} , and (b) $E_{\text{even}}^{\text{th}}$.

is fulfilled, which does not occur for E_{\max}^{th} . There is, however, always an energy $E_{\text{even}}^{\text{th}}$ for which this condition is fulfilled, and which are listed in the last column of Table 4. The values of new R , displayed in the lower panel of Fig. 5, are not very different from the previous values shown in the same figure. However, the value of the parameter a and, consequently, the ratio Γ_2^0/Γ_p^0 , is quite different now resembling those obtained by FINUDA, as can be seen from row C in Table 5. This agreement is somewhat surprising and we can not draw any conclusion from it. One has just learned that: (i) a relatively small modification of the partition energies (from E_{\max}^{th} to $E_{\text{even}}^{\text{th}}$) can lead to significantly different results for Γ_2^0/Γ_p^0 , and (ii) a relatively sizeable modification of the partition energies (from E_{\max}^{FINUDA} to $E_{\text{even}}^{\text{th}}$) can lead to quite similar results for Γ_2^0/Γ_p^0 .

It would be valuable to find the physical meaning of the fitting parameter b , which is different in the three cases discussed above. In this regard, how to arrive at (22) from (21) is not a trivial issue. One possibility is to neglect the last term in the denominator of (21), arguing, as was done in Ref.,²⁴ that the FSIs tend to remove protons from the high energy part of the spectrum ($N_{FSI}^> < 0$) while filling the low energy region ($N_{FSI}^< > 0$), with the net result that $N_{FSI} = N_{FSI}^< + N_{FSI}^> \cong 0$. Therefore

$$R \cong a + \frac{N_{FSI}^<}{(1 + \Gamma_2^0/\Gamma_p^0)N_p^0},$$

which, when compared with (22), yields

$$N_{FSI}^< \cong bAN_p^0 \left(1 + \frac{\Gamma_2^0}{\Gamma_p^0} \right) \sim bAN_p^0, \quad (25)$$

since the factor $1 + \Gamma_2^0/\Gamma_p^0 < 1.5$ is unsubstantial for a qualitative discussion. At first glance, the last equation appears reasonable because the effect of the FSIs should increase with A . But, since $b = 0.009 \pm 0.013$, it turns out that $N_{FSI}^</math>/ $N_p^0 \sim 0.01A$. Such a small amount of FSIs looks unrealistic. It is even more difficult to interpret physically the negative values of b that we obtain in cases B and C. Evidently, the fact that the IPSM is unable to reproduce the low-energy spectra in no way affects the previous discussion of Γ_2^0/Γ_p^0 .$

A different derivation of the $2N$ branching ratio has been done at FINUDA quite recently,⁶⁸ based on the analysis of the (π^-, p, n) triple coincidence events, and a χ^2 fit similar to (22). The new result, $\Gamma_2^0/\Gamma_{NM}^0 = 0.21 \pm 0.10$, is consistent within the errors with the previously obtained value,²⁴ as well as with our result. Only the sum of events from all hypernuclear species are exhibited in this work, without presenting data for individual proton spectra, which would allow us to do a reanalysis similar to that done above.

6. Summary and Conclusions

Proton kinetic energy spectra of ${}^5_{\Lambda}\text{He}$, ${}^7_{\Lambda}\text{Li}$, ${}^9_{\Lambda}\text{Be}$, ${}^{11}_{\Lambda}\text{B}$, ${}^{12}_{\Lambda}\text{C}$, ${}^{13}_{\Lambda}\text{C}$, ${}^{15}_{\Lambda}\text{N}$ and ${}^{16}_{\Lambda}\text{O}$, measured by FINUDA a few years ago,²⁴ were evaluated theoretically for the first time. We conclude that, in all the cases, the magnitudes of the spectra strongly depend on the parameterization that is used for the transition potential, while their shapes are very similar and independent of the transition mechanism. This statement, like all statements made in this work, do not depend at all on the inclusion or non-inclusion of the FSIs and $2N$ -NM channel in the nuclear model.

It is explained in detail in Sec. 2 that our method for comparing the theory with experiment is radically different from the procedure followed by other researchers. In particular:

- The equations (4) have never been used so far by any other group. These relations show that, to evaluate the decay rates, it is essential to know the number of produced hypernuclei N_W , which is not available in the literature.
- We focus our attention on measured transition probabilities Γ_N , and Γ_{nN} , instead of comparing bare quantities Γ_p^0 , Γ_n^0 , Γ_{np}^0 , *etc*, which are extracted from the experiments by making assumptions and approximations that are often questionable.
- The difference with other studies can be immediately seen by facing our Eq. (14) with [36, Eq. (7)].
- But, what is really important is that the method proposed here imposes more constraint in comparing theory with data, allowing us to examine more clearly

the decay mechanism regardless of the importance of FSIs and the 2N-NM channel.

Despite the lack of direct information about the N_W -values, we have been able to estimate these observables for ${}^5_{\Lambda}\text{He}$, ${}^7_{\Lambda}\text{Li}$, and ${}^{12}_{\Lambda}\text{C}$ hypernuclei from the ratios R_p presented in Ref.²² (The physical meaning of this ratio is also clarified.) In this way, we obtain in Sec. 3 some very useful information on the transition potential. In fact, from Figs. 2 and 3 and Table 1, we conclude that:

- The IPSM reproduces correctly the shapes of all proton kinetic energy spectra $S_p(E_p)$ at medium and high energies ($E_p \gtrsim 40$ MeV), including the Q -value, which is around 115 – 135 MeV. The latter could indicate that the residual nucleus $A-2(Z-1)$ is emitted mainly in the ground state.
- This simple model also reproduces fairly well the magnitudes of the spectra at these energies when the soft $\pi + K$ potential is used to describe the NMWD. In no way do we claim that this is the "true" physics, but we believe that it might be worth pursuing this direction, especially considering that the model is able to explain satisfactorily the NM decay rates Γ_p and Γ_n of the s-shell hypernuclei.^{8,9}
- The measured transition rates, Γ_p , the same as the corresponding spectral densities $S_p(E_p)$ for $E_p \gtrsim 40$ MeV, are significantly overestimated by the present theoretical calculations when the standard parametrization for the transition potential is used. In doing this comparison, one should keep in mind that, while the calculations refer to the 1N-NM decay mode only, the measured rates include also the 2N-NM decay channel and the effects of FSIs, and therefore the latter should always be larger. This happens only for the soft $\pi + K$ exchange potential.
- It is difficult to reconcile the FINUDA data with the theory based on the $\pi + 2\pi/\rho + 2\pi/\sigma + \omega + K + \rho\pi/a_1 + \sigma\pi/a_1$ exchange potential.¹⁷

We strongly believe that, in recent theoretical calculations,^{36,38} which include both the 2N-NM decay channel, and the FSIs, they would have arrived at very similar conclusions if the comparison with experimental data have been made in the manner proposed here.

Since the calculated spectra only involve the 1N-NM channel, the differences between them and the experimental spectra, both with respect to the magnitude and in relation to the energy distribution, can indicate which other degrees of freedom are important (2N-NM channel, FSIs, *etc*). Our plan of action is to add them to 1N-NM, when necessary, in order to successfully reproduce the experiments.

With regard to the FINUDA method²⁴ to determine the 2N-NM decay rate, based on the assumption that the 1N-NM strength of the kinetic proton spectra is equally distributed in the low and high energies, we conclude that:

- The proposed method is very sensitive to the energies that separate these two regions, and these energies can not be determined experimentally.

- The separation done in Ref.²⁴ is not supported by any firm physical argument.
- It is necessary to resort to theoretical models to establish the partition energies; the IPSM is very suitable for this purpose.
- Both theoretical sets of partition energies ($E_{\max}^{\text{th}}, E_{\text{even}}^{\text{th}}$) differ from the FINUDA result (E_{\max}^{FINUDA}), not only in magnitudes but also with regards to the mass-number dependence: E_{\max}^{th} and $E_{\text{even}}^{\text{th}}$ decrease with A , because the experimental single-particle energies increase; meanwhile, no reasonable explanation exists for the opposite behavior of E_{\max}^{FINUDA} .
- In spite of the above mentioned differences, all three sets of partition energies yield similar results for the parameter a and therefore for the ratio Γ_2^0/Γ_p^0 . This indicates that the behavior with A of the partition energies does not play a crucial role, and is consistent with a recent proposal to approximate them by a rather constant value of $\lesssim 80$ MeV.⁶⁷
- Physical interpretation of the FINUDA parameter b is a point at issue, not only for being very small, but also because it is negative in our analysis, as well as in the a new study⁶⁸ of the contribution of the $2N$ -NM channel employing the same method. Although suffering from large errors, its small value inevitably leads to the conclusion that the FSIs are very small, and that, therefore, the low-energy proton spectra dominantly comes from the $2N$ -NM decay. It is very hard to understand this fact, and the only alternative possibility is that the basic approach (22) was incorrect.

Final remarks:

- (1) As stated in the beginning, our purpose was not to reproduce the experimental data, but to discover out what the proton kinetic energy spectra can tell us about the weak hypernuclear interaction. To account for the low energy data of the kinetic energy spectra, it is imperative to consider the FSIs. For the time being, we are working on this issue by employing an improved version of the CRISP internuclear cascade model⁶⁹ used previously to describe ${}_{\Lambda}^{12}\text{C}$.^{43,44} Moreover, a complete theoretical description must also include a judicious estimate of the effect of the $2N$ -NM decay channel. So far, this has been done only in the context of FGM,^{36,38} and it would be interesting to know what the SM can tell us about this process. In fact, for quite some time, we have been involved in the development of a corresponding theoretical formalism and numerical codes.⁷⁰
- (2) To study the FSIs and the $2N$ -NM decay, it is indispensable to understand first the $1N$ -NM-decay dynamics. In our opinion, the SM could be a very useful tool to achieve this goal. For instance, the SM spectra are the main ingredients for establishing the initial conditions for the FSIs within the many-body multi-collision Monte Carlo cascade scheme.^{43,44} On the other hand, from Fig. 1, it is self-evident that the diagram a) plays the principal role within the diagram b) representing the $2N$ -NM decay mode.

- (3) New experimental developments will be very welcome, such as: i) Angular correlation of np and nn pairs to determine the Γ_{np} and Γ_{nn} rates, which have been measured so far only by KEK³⁴ in ${}^{12}_{\Lambda}\text{C}$, and ii) Triple (p, n, n) , and (p, p, n) coincidence detections for direct measurement of Γ_{pn} , and Γ_{pp} , as suggested previously.⁶⁵ The first steps in this direction seems to be given recently in Ref.⁶⁷
- (4) To complete Figs. 2 and 3, we need the N_W -values for ${}^9_{\Lambda}\text{Be}$, ${}^{11}_{\Lambda}\text{B}$, ${}^{13}_{\Lambda}\text{C}$, ${}^{15}_{\Lambda}\text{N}$ and ${}^{16}_{\Lambda}\text{O}$ hypernuclei. Hopefully, these numbers will soon be available for public use. Needless to point out that, otherwise, the proton kinetic energy spectra measured by FINUDA²⁴ are of little use to study the NMWD dynamics. They only can be exploited to discuss the decay kinematics through the analysis of the FSIs and the $2N$ -NM decay mode.

Acknowledgements

FK is supported by by Argentinean agencies CONICET (PIP 0377) and FON-CYT (PICT-2010-2680), as well as by the Brazilian agency FAPESP (CONTRACT 2013/01790-5). We are very grateful to Dr. Gianni Garbarino and Dr. Airtton Deppman for very enlightening discussions and to Dr. Wayne Allan Seale for the careful and critical reading of the manuscript.

References

1. W.M. Alberico, G. Garbarino, Phys. Rep. **369**, (2002) 1.
2. V. G. J. Stoks, R. A. M. Klomp, C. P. F. Terheggen, and J. J. de Swart, Phys. Rev. C **49**, (1994) 2950.
3. J. F. Dubach, G. B. Feldman, B. R. Holstein, L. de la Torre, Ann. Phys. (N.Y.) **249**, (1996) 146.
4. A. Parreño, A. Ramos, and C. Bennhold, Phys. Rev. C **56**, (1997) 339.
5. R. Bockmann, C. Hanhart, O. Krehl, S. Krewald, and J. Speth, Phys. Rev. C **60**, (1999) 055212.
6. K. Nakayama, private communication (2012).
7. J. Ryckebusch, M. Vanderhaeghen, L. Macheuil, and M. Waroquier, Nucl. Phys. A **568**, (1994) 828.
8. E. Bauer, A.P. Galeão, M. Hussein, F. Krmpotić, and J.D. Parker, Phys. Lett. B **674**, (2009) 103.
9. F. Krmpotić, Few-Body Syst **55**, (2014) 219.
10. F. Krmpotić, Phys. Rev. C **82**, (2010) 055204.
11. A. Parreño, A. Ramos, Phys. Rev. C **65**, (2001) 015204.
12. K. Sasaki, T. Inoue, and M. Oka, Nucl.Phys. A **669**, (2000) 331; Erratum-ibid. A **678**, (2000) 455.
13. K. Sasaki, T. Inoue, and M. Oka, Nucl. Phys. A **707**, (2002) 477.
14. A. Parreño, C Bennhold, and B. R. Holstein, Phys. Rev. C **70**, (2004) 051601.
15. C. Chumillas, G. Garbarino, A. Parreño, and A. Ramos, Phys. Lett. B **657**, (2007) 180.
16. K. Itonaga, T. Motoba, T. Ueda, and Th.A. Rijken, Phys. Rev. C **77**, (2008) 044605.
17. K. Itonaga, T. Motoba, Prog. Theor. Phys. Suppl. **185**, (2010) 252.

24 *Franjo Krmpotić and Cláudio De Conti*

18. M. Ruderman and R. Karplus, Phys. Rev. **102**, (1956) 247.
19. W.M. Alberico, A. De Pace, M. Ericson, and A. Molinar, Phys. Lett. B **256**, (1991) 134.
20. A. Ramos, E. Oset and L.L. Salcedo, Phys. Rev. C **50**, (1994) 2314.
21. M. J. Kim, *et al.*, Phys. Rev. Lett. **103**, (2009) 182502 .
22. M. Agnello *et al.*, Nucl. Phys. A **804**, (2008) 151.
23. M. Agnello *et al.*, Phys. Lett. B **681**, (2009) 139.
24. M. Agnello *et al.*, Phys. Lett. B **685**, (2010) 247.
25. E. Bauer, and G. Garbarino, Nucl. Phys. A **828**, (2009) 29.
26. J. D. Parker *et al.*, Phys. Rev. C **76**, (2007) 035501.
27. J.J. Szymanski *et al.*, Phys. Rev. C **43**, (1991) 849.
28. H. Noumi *et al.*, Phys. Rev. C **52**, (1995) 2936.
29. J. H. Kim *et al.*, Phys. Rev. C **68**, (2003) 065201.
30. S. Okada *et al.*, Phys. Lett. B **597**, (2004) 249.
31. S. Okada *et al.*, Nucl. Phys. A **752** , (2005) 196.
32. H. Ota *et al.*, Nucl. Phys. A **754** , (2005) 157c.
33. B. H. Kang *et al.*, Phys. Rev. Lett. **96**, (2006) 062301.
34. M. J. Kim *et al.*, Phys. Lett. B **641**, (2006) 28.
35. H. Bhang *et al.*, Eur. Phys. J. A **33**, (2007) 259.
36. E. Bauer, G. Garbarino, A. Parreño, and A. Ramos, Nucl. Phys. A **836**, (2010) 199.
37. E. Bauer, and G. Garbarino, Phys. Rev. C **81**, (2010) 064315.
38. E. Bauer, and G. Garbarino, Phys. Lett. B **698**, (2011) 306.
39. O. Benhar, Nucl. Phys. B (Proc. Suppl.) **159**, (2006) 168.
40. A. Meucci, C. Giusti, M. Vorabbi, Phys. Rev. D **88** 013006.
41. H. F. Schopper , *Weak Interactions and Nuclear β -decay* (North-Holland Publ. Co., Amsterdam, 1966).
42. A. Ramos, M. J. Vicente-Vacas, and E. Oset, Phys. Rev. C **55**, 735 (1997);C **66**, 039903 (2002)(E).
43. I. Gonzalez *et al.*, J. Phys. Conf. Ser. **312**, (2011) 022017.
44. I. Gonzalez, C. Barbero, A. Deppman, S. Duarte, F. Krmpotić, O. Rodriguez, J. Phys. G: Nucl. Part. Phys. **38**, (2011) 115105.
45. A. Deppman, S. B. Duarte, G. Silva, O. A. P. Tavares, S. Anefalos, J. D. T. Arruda-Neto, T. Rodrigues J. Phys. G: Nucl. Part. Phys. **30** 1991.
46. A. Deppman, G. Silva, S. Anefalos, S. B. Duarte, F. Garcia, F. H. Hisamoto, O. A. P. Tavares Phys. Rev. C **73** 064607.
47. A. Deppman, O. A. P. Tavares , S. B. Duarte, E. C. Oliveira, J. D. T. Arruda-Neto, S. de Pina, V. Likhachev, O. Rodriguez, J. Mesa, M. Goncalves Phys. Rev. Lett. **87** 82701
48. O. A. P. Tavares , S. B. Duarte, V. Likhachev, A. Deppman J. Phys. G: Nucl. Part. Phys. **30** 37.
49. G. Garbarino, A. Parreño, and A. Ramos, Phys. Rev. C **69**, (2004) 054603.
50. E. Botta, *Weak Decay of Hypernuclei (FINUDA, KEK) Experiment*, SPHERE School + 22nd Indian-Summer School of Physics STRANGENESS NUCLEAR PHYSICS, Rez/Prague, Czech Republic (2010).
51. D. P. Heddle and L.S . Kisslinger, Phys. Rev. C **33**, (1986) 608.
52. J. Cohen, Prog. Part. Nucl. Phys. **25**, (1990) 139.
53. C. Barbero, D. Horvat, F. Krmpotić, T. T. S. Kuo, Z. Narančić, and D. Tadić, Phys. Rev. C **66**, (2002) 055209.
54. F. Krmpotić, and D. Tadić, Braz. J. Phys. **33**, (2003) 187.
55. C. Barbero, C. De Conti, A. P. Galeão and F. Krmpotić, Nucl. Phys. A **726**, (2003)

- 267.
56. C. Barbero, A. P. Galeão, and F. Krmpotić, *Phys. Rev. C* **76**, (2007) 054321.
 57. C. Barbero, A. P. Galeão, M. S. Hussein, and F. Krmpotić, *Phys. Rev. C* **78**, (2008) 044312; Erratum-ibid. 059901(E).
 58. E. Bauer, A. P. Galeão, M. S. Hussein and F. Krmpotić, *Nucl. Phys. A* **834**, (2010) 599c.
 59. F. Krmpotić, A. P. Galeão, and M.S. Hussein, *AIP Conf. Proc.* **1245**, (2010) 51.
 60. F. Krmpotić, A. Samana, and A. Mariano, *Phys. Rev. C* **71**, (2005) 044319 .
 61. E. Bauer, *Nucl. Phys. A* **818**, (2009) 174.
 62. TUNL Nuclear Data Project, www.tunl.duke.edu/nucldata/ (2012).
 63. D.J. Millener, *Lecture Notes in Physics* **724** (Springer, 2007) 31.
 64. G. Garbarino, A. Parreño and A. Ramos, *Phys. Rev. Lett.* **91**, (2003) 112501.
 65. C. de Conti, A. Deppman, F. Krmpotić, arXiv:1202.4223.
 66. G. Jacob and T. A. J. Maris, *Rev. Mod. Phys.* **45**, (1973) 6.
 67. S. Bufalino, *Nucl. Phys. A* **914**, (2013) 160.
 68. M. Agnello *et al.*, *Phys. Lett. B* **701**, (2011) 556.
 69. C. Barbero, A. Deppman, S. Duarte, F. Krmpotić, in preparation.
 70. C. Barbero, E. Bauer, C. De Conti, A. P. Galeão and F. Krmpotić, in preparation.